Atomic-level Drug Substance and Polymer Interaction in Posaconazole Amorphous Solid Dispersion from Solid-State NMR

Xingyu Lu[1,§], Mingyue Li[1,§], Chengbin Huang[1,§], Michael B. Lowinger[1], Wei Xu[1], Lian Yu[2], Stephen R. Byrn[3], Allen C. Templeton[1], and Yongchao Su[1,3,4*]

[1] Pharmaceutical Sciences, Merck & Co., Inc., Kenilworth, NJ 07033, United States

[2] School of Pharmacy and Department of Chemistry, University of Wisconsin−Madison, Madison, WI 53705, United States

[3] Department of Industrial and Physical Pharmacy, College of Pharmacy, Purdue University, Indiana 47907, United States

[4] Division of Molecular Pharmaceutics and Drug Delivery, College of Pharmacy, The University of Texas at Austin, Austin, Texas 78712, United States

Revised for *Molecular Pharmaceutics*

April 25th, 2020

[§]X. L., M. L. and C. H. have equal contribution.

* Corresponding author: Y. S.: yongchao.su@merck.com

Table of Content (TOC) Figure

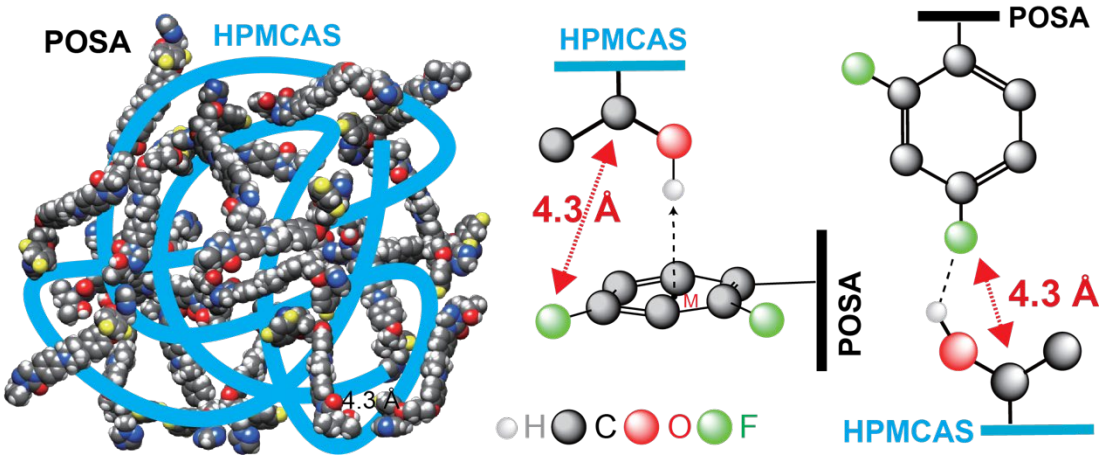

Abstract

Despite the wide utilization of amorphous solid dispersions (ASDs) for formulating poorly water-soluble drugs, fundamental understanding of the structural basis behind their stability and dissolution behavior is limited. This is largely due to the lack of high-resolution structural tools for investigating multi-component and amorphous systems in the solid state. In this study, we present what is likely the first publication quantifying the molecular interaction between drug and polymer in ASDs at an angstrom level by utilizing ^{19}F magic angle spinning (MAS) nuclear magnetic resonance (NMR) techniques. A variant of ^{19}F-^{13}C Rotational Echo and Double Resonance (REDOR) technique was developed to quantify interatomic distances by implementing a super-cycled symmetry-based recoupling schedule and synchronized simultaneous detection. We successfully deployed the technique to identify "head-to-head" and "head-to-tail" packing of crystalline posaconazole (POSA). To probe molecular interactions between POSA and hypromellose acetate succinate (HPMCAS) in the dispersion, as a major goal of this study, two-dimensional (2D) ^{1}H-^{19}F correlation experiments were performed. The approach facilitated observation of inter-molecular hydrogen-to-fluorine contacts between the hydroxyl group of the polymer and the difluorophenyl group of the drug substance. Atomic distance measurement, utilizing the developed ^{19}F-^{13}C REDOR technique, revealed the close proximity of $^{13}C_{OH}$-^{19}F at 4.3 Å. Numerical modeling analysis suggested a possible hydrogen bonding interaction between the polymer O-H group as an acceptor and POSA fluorine (O-H···F) or difluorophenyl ring (O-H···Ph) as a donor. These ^{19}F MAS NMR techniques, including 2D ^{19}F-^{1}H hetero-nuclear correlation and ^{19}F-^{13}C atomic distance measurement, may shed light on the nature (*i.e.* type and strength) of drug-polymer interactions in ASDs and offers a new high-resolution analytical protocol for probing the microstructure of amorphous pharmaceutical materials.

1. Introduction

In the previous decade, approximately 40% of marketed drug products and 60% of new molecular entities suffered from the poor aqueous solubility, belonging to Class II and IV of the biopharmaceutical classification system (BCS).[1] Amorphous solid dispersions (ASDs), molecular mixtures of active pharmaceutical ingredients (APIs) and polymers, have emerged as a key enabling formulation approach to improve solubility and oral bioavailability of poorly water-soluble APIs.[2-4] A key risk in the development of ASDs lies in the use of the amorphous form, which is thermodynamically unstable and tends to crystallize.[5] This risk is typically mitigated by the addition of polymer additives, which may inhibit drug crystallization and improve the physical stability of ASDs.[6, 7] However, the *a priori* rational selection of polymer capable of inhibiting drug crystallization is poorly understood. It has generally been proposed that inter-molecular interactions between drug and polymer can explain the ability of some polymers to effectively inhibit drug crystallization, resulting in improved physical stability and oral bioavailability. Taylor and coworkers observed a correlation between drug-polymer interactions and surface enrichment in ledipasvir-copovidone dispersions, suggesting that it impacted drug release profiles.[3] Most recently, API and polymer interactions between indomethacin (IND) and indomethacin methyl ester (INDester) as model drugs, and poly(vinylpyrrolidone-co-vinyl acetate) (PVPVA) have been investigated by attenuated total reflectance-FTIR (ATR-FTIR) spectroscopy.[8] The comparison suggests that hydrogen bonding interaction plays a critical role to impact the initial dissolution rate of ASDs. Additionally, many studies reported a general correlation between drug-polymer interactions and the polymers' inhibitory effect on drug crystallization.[9-14] Despite the apparently critical role of API-polymer molecular interactions in the stability and bioavailability performance of ASDs, it is currently technically challenging to investigate structural details in ASDs. The complexity of molecular interaction and the nature of amorphous materials require high-resolution structural characterization.

A broad range of analytical techniques have been utilized to characterize ASDs.[15] For example, powder X-ray diffraction (PXRD) detects and quantifies crystallinity;[16] transmission electron microscopy (TEM)[17] and atomic force microscopy (AFM)[18] probe morphological characteristics; infrared spectroscopy (IR)[19], Raman spectroscopy[20], X-ray photoelectron spectroscopy (XPS)[21], and solid-state nuclear magnetic resonance (ssNMR)[11] have been used to probe molecular interactions in ASDs. Pioneering in the study of drug-polymer interactions in ASDs, Taylor and Zografi employed IR and Raman spectroscopy to characterize molecular interactions in indomethacin-polyvinylpyrrolidone (PVP) and lyophilized trehalose/maltose/raffinose-PVP amorphous dispersions.[19, 20] Since then, IR and Raman spectroscopy have been increasingly utilized to explore drug-polymer interactions in various ASDs, *e.g.*, in felodipine-PVP dispersions by Marsac *et al.*[22], in curcumin-hydrophilic polymer dispersions by Meng *et al.*[23], and in

nifedipine-polymer dispersions by Kothari *et al.*[9]. It has been shown that molecular interactions between drug and polymer correlate with the physical stability and miscibility of ASDs.[9, 22, 23] Strong inter-molecular interactions greatly improve the resistance of amorphous API to recrystallization in ASDs[9]. Recently, high-energy X-ray scattering and pair distribution function (PDF) analysis were applied to tentatively resolve drug-drug and drug-polymer interactions in lapatinib dispersions[24]. By applying X-ray photoelectron spectroscopy to study inter-molecular interactions in ledipasvir-copovidone ASDs, Taylor and coworkers found that potential hydrogen bonding between the fluorine associated with drug molecules and amine groups of polymers disrupts drug-drug interaction at drug loadings below 5% (w/w), playing a beneficial role in affecting the drug release profile.[21] However, detailed structural information of molecular interactions are still lacking, limiting understanding of the pattern and strength of drug-polymer interactions and their resultant influence on drug dissolution and physical stability behavior.[23, 25, 26] For example, vibrational spectroscopy can qualitatively characterize the API and polymer interaction in ASDs by evaluating frequency changes of the vibration of chemical bonds, but might lack the quantitative capability to identify the strength of interaction.[23] In recent years, 2D MAS NMR homo- and hetero-nuclear correlation experiments were employed to identify the nature of the interaction at molecular level. [12, 27-31] These 2D methods probe the drug-polymer interaction by measuring their proximity and therefore offer more sensitive and robust characterization than one-dimensional (1D) ^{13}C and ^{15}N cross polarization (CP) techniques, as elaborated previously.[27] For example, in our prior study of posaconazole (POSA) and hypromellose acetate succinate (HPMCAS) ASDs, 2D ^{1}H-^{13}C hetero-nuclear correlation (HETCOR) experiments revealed two types of POSA-HPMCAS inter-molecular interactions: a hydrogen bond between the POSA triazole ring and the HPMCAS hydroxyl group; and an electrostatic interaction between the POSA carbonyl group and the HPMCAS carboxyl group. They were identified by inter-molecular correlation peaks in 2D spectra of ASDs. A third type of interaction, a hydrogen bonding between the POSA fluorine and a hydroxy proton of HPMCAS has been proposed based on indirect observation of interactions between fluorine and aliphatic carbons of HPMCAS neighbored to the hydroxyl group in 1D ^{19}F-^{13}C CP spectra. However, high resolution details (*e.g.*, drug-polymer proximity representing the strength of interaction) are still missing. Techniques that can provide distance restraints of an amorphous molecule at molecular level are largely absent. For example, the amorphous nature of ASDs hinders the application of conventional diffraction techniques for structural characterization. Therefore, it is rare to see examples of high-resolution structural characterization of amorphous pharmaceuticals.

Solid-state NMR (ssNMR) spectroscopy is a powerful technique to probe molecular structure by measuring atomic distances in crystalline[32] and non-crystalline materials[33], peptides and proteins[34], and complex biological systems[35]. For example, Rotational-echo double resonance (REDOR) NMR is the most

widely applied method for measuring the strength of dipolar coupling between two spin-1/2 nuclei, and thereby determining molecular distances. REDOR utilizes rotor-synchronized pulses to recouple short- and long-range dipolar couplings between pairs of hetero-nuclear spins, which is otherwise averaged by magic angle spinning[36]. REDOR measurements have been widely employed to measure distances among ^{1}H, ^{2}H, ^{13}C, ^{15}N, ^{19}F and ^{31}P spins to obtain critical constraints for structural determination[37-43]. ^{19}F has an inherently high gyromagnetic ratio and high natural abundance. Therefore, the application of ^{19}F for assessing distance can enhance the sensitivity and increase the range of measurable inter-atomic distances[44-46]. In addition, about 30% of pharmaceutical compounds are fluorinated in order to modulate the properties of drug molecules[47], and fluorine is usually absent from polymeric excipients[48]. Therefore, the use of ^{19}F-^{13}C REDOR for distance measurements in ASDs has a great potential to probe inter-molecular distance between API and polymer. Semi-quantitative structural analysis using ^{19}F-^{13}C HETCOR spectra has been previously demonstrated in polymers, pure APIs, and ASDs. Spiess *et al*. described the application of ^{19}F-^{13}C HETCOR for structural assignments in polymers[49]. Dybowski and coworkers utilized ^{19}F-^{13}C HETCOR to help determine a polymorph of atorvastatin[50]. Recently, by utilizing modern ultrafast MAS probes, 2D and 3D experiments of hetero-nuclear correlation between ^{19}F and ^{13}C or ^{1}H were applied to detect new molecular interactions in ASDs[27, 29, 51, 52]. Quantitative determination of inter-nuclear proximities between ^{19}F and other nuclei such as ^{1}H, ^{15}N, ^{31}P and ^{13}C has the potential to provide rich structural details on small molecules and proteins and techniques have greatly advanced over the past few decades[52-58]. In 1993, Burns and Hagaman demonstrated the utility of ^{19}F-^{13}C REDOR for identifying the local structure of organofluorides[54]. ^{19}F-^{13}C REDOR has been used to measure a distance of up to 12 Å on [^{19}F]oritavancin-peptidoglycan complexes[55]. Recently, Mei and her coworkers developed a 2D ^{13}C-^{13}C resolved ^{19}F-^{13}C REDOR experiment to measure multiple long-range distances in a 56-residue protein GB1, tripeptide formyl-MLF, and membrane-bound influenza B M2 transmembrane peptide[52].

In this study, we developed and utilized ^{19}F MAS NMR techniques to explore drug-polymer interactions by measuring inter-molecular distances to uncover the nature of molecular interaction in a pharmaceutical ASD. We selected a fluorinated drug molecule posaconazole (POSA) as a model compound, and the commonly used ASD polymer hypromellose acetate succinate to prepare a POSA-HPMCAS amorphous solid dispersion using a melt-quenching method. The structural details of crystalline POSA, including “head-to-head” and “head-to-tail” packings, were qualitatively explored by ^{19}F-^{13}C cross polarization build-up curves and quantitatively captured by an improved ^{19}F-^{13}C Rotational Echo and Double Resonance technique. Our quantitative REDOR method was then applied to the POSA-HPMCAS dispersion, and effectively determined the type of molecular interactions with the aid of geometric calculations.

2. Materials and Methods

Materials

Crystalline POSA was obtained from Merck & Co., Inc. (Kenilworth, NJ, USA). The schematic molecular structure of POSA with atoms numbered is shown in **Figure 1A**. Isotopically ^{13}C-C44 labeled POSA was synthesized for site-specific investigation. Hypromellose acetate succinate (HPMCAS) was kindly provided by Ashland, Inc. (Wilmington, DE, USA) and its molecular structure is shown in **Figure 1B**. Both crystalline POSA and HPMCAS were utilized without further purification.

Preparation of Amorphous Materials

To facilitate the dissolution of crystalline POSA into HPMCAS matrix, the physical mixture was initially blended and then underwent cryomilling. A physical mixture of 30 wt % POSA and 70 wt % HPMCAS was cryomilled (SPEX CertiPrep 6750) at 10 Hz for five cycles using liquid nitrogen as a coolant. Each cryomilling cycle was 2 minutes, followed by a 2-minute cooldown to prevent sample overheating. The cryomilled sample was then melted at 453 K for 20 minutes and quenched to room temperature, in order to prepare the POSA-HPMCAS amorphous solid dispersion. To easily transfer materials into NMR rotors, the melt-quenched ASD was underwent grinding using a mortar and pestle. The amorphous POSA (without polymer) sample was prepared using the same protocol, except the cryomilling step. Thermogravimetric analysis (TGA) confirms the thermal stability of POSA up to 473 K. Differential scanning calorimetry (DSC) measurements show the fingerprint glass transition temperature (T_g) of POSA, HPMCAS, and POSA-HPMCAS ASD are 331 K, 387 K and 360 K, respectively, as shown in **Figure S4**.[27] Besides, ^{13}C and ^{19}F spectra (data not shown) before and after ssNMR experiments remain identical, which further confirms the stability of the samples in this study.

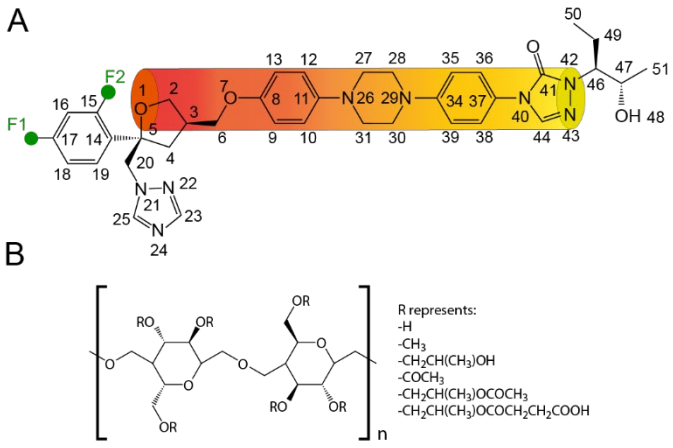

Figure 1. Schematic structures of (A) posaconazole and (B) hypromellose acetate succinate. Note that the orange column in (A) represents the major molecular axis of the POSA molecule.

Solid-state NMR spectroscopy

MAS NMR experiments were performed on a 9.4 T Bruker AVANCE III HD spectrometer with Larmor frequencies of 400.13 and 100.63 MHz for ^{1}H and ^{13}C nuclei, respectively, in the Biopharmaceutical NMR Laboratory (BNL) of Preclinical Development at Merck Research Laboratories (Merck & Co., Inc. West Point, PA). A commercial Bruker 4 mm HFX MAS probe in triple-resonance mode was used for all experiments. Typical ^{1}H, ^{19}F, and ^{13}C 90° pulses were 2.5 μs, 2.5 μs, and 3.0 μs, respectively. All experiments were conducted at a MAS frequency of 12 kHz, except the 1D ^{19}F high power decoupling experiment which was acquired at 5 kHz. Experimental data were processed using Bruker TopSpin applied with Gaussian and Qsine-bell lineshape functions. ^{1}H and ^{13}C chemical shifts were referenced to tetramethylsilane (TMS). ^{19}F spectra were referenced to Teflon at -122 ppm. During the 1D ^{1}H-^{13}C cross polarization (CP) MAS experiments, the contact time for ramped CP transfer was 2.0 ms and a recycle delay of 2.0 s was used. Due to the availability of two high-power amplifiers in BNL, SPINAL64 hetero-nuclear decoupling with a radio-frequency (RF) power of 100 kHz was simultaneously applied on both ^{1}H and ^{19}F channels, which significantly improved the spectral resolution of carbons (C15 and C17 in **Figure 1A**) directly bonded to the fluorine in POSA. To obtain CP build-up curves for semi-quantitative ^{19}F-^{13}C distance analysis, 1D ^{19}F-^{13}C CP spectra with contact times of 0.25 ms, 0.75 ms and 1.5 ms were acquired. Each spectrum was collected using 4096 number of scans. A recycle delay of 20.0 s was used for full magnetization recovery, giving approximately 24-hr experimental time for each spectrum. The ^{19}F CP spin-lock pulse was linearly ramped from 90 to 110%. 2D ^{1}H-^{19}F hetero-nuclear correlation (HETCOR) experiments were conducted using a contact time of 5 ms. These 2D spectra were acquired with 16 points in the indirect dimension and 32 scans in the direct dimension. A recycle delay of 5.0 s between consecutive scans was used, giving approximately 0.7 hour experimental time for each 2D. Hetero-nuclear TPPM decoupling with an RF field of 100 kHz was applied in the indirect proton dimension.

Rotational-echo double-resonance with supercycled symmetry-based recoupling schedule and synchronized simultaneous detection

We utilized a ^{13}C-^{19}F REDOR sequence shown in **Figure 2** employing a $SR4_1^2$ recoupling sequence and simultaneous acquisition of REDOR dephased and reference signals S and S_0, respectively, for the measurement of ^{13}C-^{19}F distance. It starts with a ^{1}H 90 degree pulse and ^{1}H-^{13}C CP to enhance ^{13}C signal sensitivity. Two $SR4_1^2$ schemes of equal duration, τ, were inserted into a spin echo. The total delay 2τ is defined as the dipolar recoupling time. The hetero-nuclear dipolar coupling is restored by applying two $SR4_1^2$ schemes and the π pulse in the middle of the sequence on the fluorine channel. The π pulse applied

on the observed nuclei ^{13}C refocuses isotropic chemical shifts. The application of the simultaneous π pulses on ^{19}F nuclei prevents the refocusing of the recoupled hetero-nuclear dipolar coupling resulting in a dephased spectrum S. In the absence of the π pulse on the ^{19}F channel, the recoupled hetero-nuclear dipolar coupling becomes refocused and gives a reference spectrum S_0. The use of the super-cycled symmetry-based recoupling sequence $SR4_1^2$ for hetero-nuclear dipolar recoupling can overcome the limitations of a classical REDOR method, which enhances robustness to radio frequency inhomogeneity and homo-nuclear dipolar interaction, and exhibits low demand on recoupling power and experimental optimization[59-61]. The application of symmetry-based REDOR (S-REDOR) has been demonstrated for inter-atomic distance measurements of ^{1}H-^{13}C, ^{13}C-^{15}N/^{14}N and ^{1}H-^{17}O spin pairs[60, 62]. The $SR4_1^2$ recoupling scheme utilizes super-cycled and rotor synchronized composite pulses employing π pulses as a basic element[59, 63]. $SR4_1^2$ requires an RF strength of twice the spinning frequency. High-power SPINAL64 decoupling is applied on ^{1}H channel during REDOR period and acquisition. Reference REDOR spectrum S_0 and dephased spectrum S are simultaneously acquired in each scan. These pseudo 2D REDOR data were acquired with 1024 scans for each t1 increment and with a total of 64 points of mixing time acquired. A recycle delay of 2.0 s between consecutive scans was used, giving approximate 37-hr experimental time for each REDOR experiment. Additional experimental parameters of ^{13}C-^{19}F REDOR experiments are included in the SI.

Numerical simulations for the REDOR sequence were performed using SIMPSON software[64]. NMR experimental parameters including magnetic field, spinning speed, RF strength and pulse length were included in the simulations. Chemical shift anisotropy of two fluorine atoms was also considered in simulations. The powder averaging was accomplished by using 2184 Euler orientations with the REPULSION algorithm[64]. S_0 and S signals are obtained without and with the π pulse on the ^{19}F channel. Simulations employing a three-spin system denoted ^{13}C-^{19}F-^{19}F were used in **Figures 5, 6 and 9**, except in **Figure 5D** and **Figure S2A**. A four-spin system (^{13}C, ^{13}C, ^{19}F and ^{19}F) was considered in **Figure 5D** due to peak overlapping of C49 and C51, and a two-spin system (^{13}C, ^{19}F) in **Figure S2A** was performed to investigate the effect of dipolar truncation. The relative orientation of inter-atomic distances was fixed at 120°. **Figure 9** compares different relative orientations of the same spin system by fixing inter-atomic distances at angles of 180° and 60°, respectively. Experimental and simulated signal fraction $(S_0\text{-}S)/S_0$ are plotted as a function of the recoupling time 2τ in **Figures 5, 6, 9 and S2**.

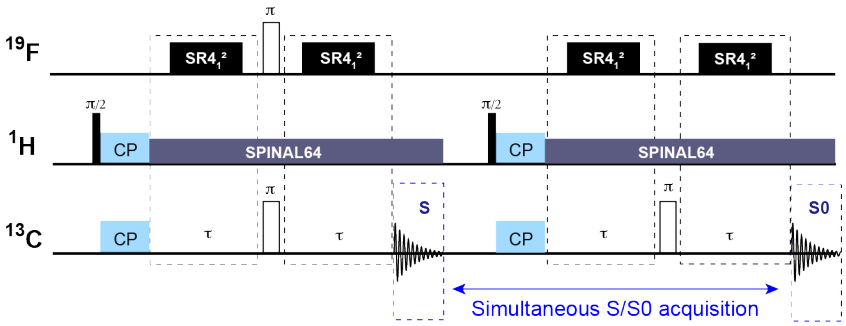

Figure 2. NMR pulse sequence of ^{13}C-^{19}F S-REDOR which recouples ^{13}C-^{19}F dipolar interactions for determining ^{13}C-^{19}F hetero-nuclear distances.

3. Results

Amorphous solid dispersions have become among the most widely applied formulation approaches to improve the oral bioavailability of BCS Class II and IV drugs[1]. Polymer screening of ASDs, including polymer type and concentration, is generally an important determinant of critical drug product quality attributes, such as bioavailability, stability and manufacturability. Several others have reported correlations between drug-polymer interactions and pharmaceutical attributes.[25,65-68] Consequently, in-depth understanding of drug-polymer interactions may inform polymer selection during formulation development by narrowing down the appropriate polymer types. In this study, POSA was utilized as a model system to investigate molecular interactions at atomic level.

3.1 Probing molecular structure from semi-quantitative ^{19}F MAS NMR

To support structural investigation of crystalline POSA and the POSA-HPMCAS dispersion, we leveraged chemical shifts of ^{13}C and ^{19}F atoms that we reported in our previous studies.[27] Briefly, ^{13}C chemical shift assignments of crystalline POSA were carried out utilizing 1D ^{13}C-edited experiments, 2D ^{13}C-detected homo- and hetero-nuclear correlation experiments following our established protocol.[69] Two fluorine atoms were unambiguously identified in a 2D ^{19}F-^{19}F homo-nuclear correlation experiment by taking advantage of their different chemical environment (*i.e.*, F1 is more shielded than the ortho-fluorine, F2). However, full chemical shift assignments of POSA in the POSA-HPMCAS dispersion were challenging due to broad spectral linewidth and peak overlapping. To unambiguously assign chemical shifts in the POSA-HPMCAS dispersion, reference materials including neat amorphous POSA and neat amorphous HPMCAS were measured by 1D and 2D ssNMR experiments[69]. The assigned chemical shifts of POSA in the POSA-HPMCAS dispersion are summarized in **Table S1** and partially illustrated in **Figure S1**. In comparison to neat amorphous POSA, most of the carbons show slight chemical shift perturbations in POSA-HPMCAS dispersion. For example, chemical shift perturbations of C41 and C44 were observed. These perturbations suggest chemical environment changes, which we propose to correspond to their

involvement in inter-molecular interactions with HPMCAS in 2D ^{1}H-^{13}C correlation experiments.[27] Although 2D correlation experiments are well established for probing inter-molecular interactions, knowledge of the strength and configuration of such interactions cannot be ascertained with this technique.

Hetero-nuclear dipolar recoupling using ^{19}F-^{13}C cross polarization (CP) has been used to semi-quantitatively evaluate ^{19}F-^{13}C distances in fluorinated materials[70, 71]. To compare inter-atomic proximities in crystalline POSA, a semi-quantitative analysis of ^{19}F-^{13}C proximities was performed using CP build-up curves. In **Figure 3A**, 1D ^{13}C-^{19}F CP MAS spectra were acquired at contact times of 1.50 ms, 0.75 ms and 0.25 ms, and a 1D ^{1}H-^{13}C CP spectrum was acquired using a long contact time (2 ms). The 1D ^{1}H-^{13}C CP spectrum exhibits all thirty-seven ^{13}C resonances of crystalline POSA, while only limited carbons are shown in 1D ^{19}F-^{13}C CP spectra and their intensity increases when acquired with longer contact times. This is because magnetization transfer from ^{19}F to ^{13}C in 1D ^{19}F-edited ^{13}C CP spectra is constrained by distances, and is favorable for only those carbons forming covalent bonds or spatially close. A short distance corresponding to a strong dipolar coupling would result in a fast ^{13}C-^{19}F CP intensity build-up rate, and vice versa. In **Figure 3B**, the CP build-up rate of fluorine to covalent-bonded C17 is faster than to C16 which is two-bonds away and to C5 at a further distance. Note that the corresponding distances labeled in **Figure 3B** are obtained from the crystallography structure[72]. The ^{19}F-^{13}C build-up curve provides a semi-quantitative method to probe inter-nuclear ^{13}C-^{19}F distances, while a quantitative protocol to measure ^{13}C-^{19}F distances is still required for obtaining molecular details, *e.g.* bond length of intermolecular contacts.

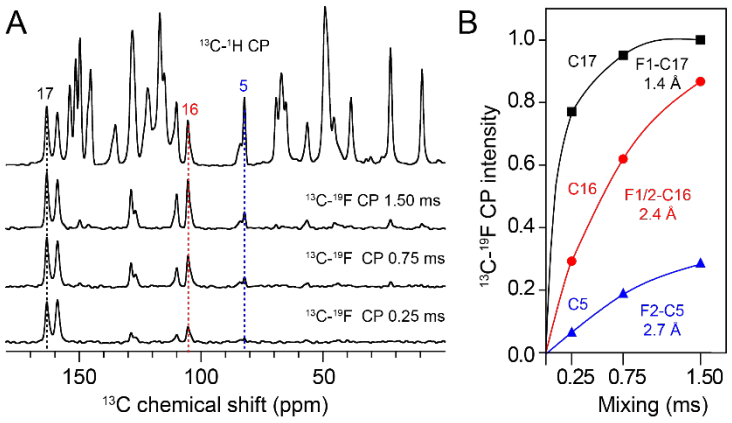

Figure 3. Semi-quantitative evaluation of ^{13}C-^{19}F distances in crystalline POSA from ^{13}C-^{19}F CP build-up curves. (A) 1D ^{13}C-^{1}H CP MAS spectrum at a contact time of 2 ms and 1D ^{13}C-^{19}F CP MAS spectra acquired at contact times of 1.50 ms, 0.75 ms and 0.25 ms; (B) CP build-up curves obtained by plotting peak intensities of ^{13}C-^{19}F CP MAS spectra as a function of contact time. Note that the bond distances are obtained from a previous crystallography study[72].

3.2 Atomic ^{13}C-^{19}F distance measurements in crystalline POSA

Since its introduction in 1989, REDOR has been widely utilized method for measuring distances of hetero-nuclear spins. It has been most widely used to recouple dipolar couplings and measure short- and long-range distances[36]. The dipolar coupling in solid state is suppressed by magic angle spinning in a coherent manner. REDOR experiments utilize rotor-synchronized radio frequency pulses to operate on spin coordinates and reintroduce dipolar couplings, which can be used to calculate precise distances. The dipolar coupling constant, *D*, is calculated using equation 1.

$$D = {}^{\mu_0 \gamma_I \gamma_S \hbar}/_{8\pi^2 r^3} \qquad (1)$$

γ_I and γ_S are the gyromagnetic ratios of *I* and *S* nuclei; *r* is the inter-nuclear distance between the two spins; μ_0 is the magnetic constant; and $\hbar$ is the reduced Plank constant. Conventional REDOR sequences also recouple the unwanted homo-nuclear dipolar coupling between two spin 1/2 nuclei, such as ^{19}F-^{19}F dipolar coupling, which would interfere REDOR curve fitting.[61] In this study, we introduced a super-cycled symmetry-based $SR4_1^2$ sequence for recoupling hetero-nuclear dipolar couplings while suppressing ^{19}F-^{19}F homo-nuclear interactions. The REDOR sequence implemented in this study is shown in **Figure 2**. ^{13}C-^{19}F REDOR measurements were conducted in two steps to yield the reference spectrum (S_0) and the dephased spectrum (S), which were acquired without (S_0) and with (S) the central π pulse in between recoupling schemes on ^{19}F channel, respectively. In addition, to eliminate the differences of T_2 decay during the acquisition of S_0 and S, we implemented simultaneous acquisition of S_0 and S in the same scan. The time period during which dipolar coupling is recoupled by the $SR4_1^2$ sequence is termed the REDOR recoupling time (2τ in our sequence). Dipolar couplings result in signal attenuation after $SR4_1^2$ sequences when the middle π pulse is applied. Stronger dipolar couplings usually correspond to larger signal attenuation. ^{19}F-^{13}C REDOR spectra of crystalline POSA, shown in **Figure 4,** were acquired at recoupling times of 0.2 ms and 2.3 ms. The peak intensity attenuation varies for different carbon peaks, suggesting differences in their distances to fluorine atoms. An example is highlighted on the right of **Figure 4**, wherein C11 shows a negligible intensity decrease with an increment of recoupling time from 0.2 ms to 2.3 ms, while C5 displays a significant signal dephasing. This agrees well with the crystalline POSA structure, in which C5 is spatially closer to the intra-molecular fluorine atoms in the difluorophenyl ring than C11.

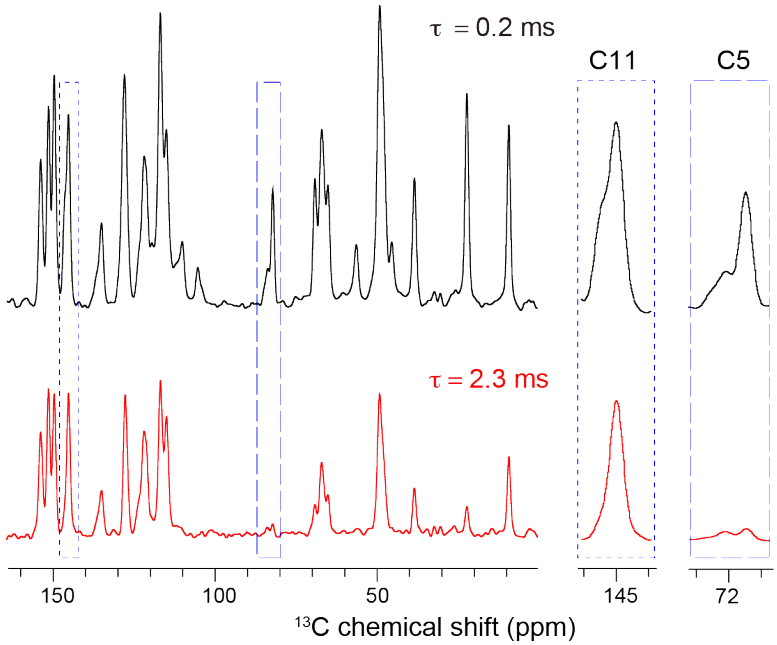

Figure 4. 1D ^{13}C-^{19}F REDOR dephased spectra of crystalline POSA at a dephasing time of 0.2 ms (top) and 2.3 ms (bottom). Zoomed spectral regions of C11 and C5 peaks are highlighted and shown on the right.

A series of 1D REDOR reference spectra, S_0, and dephasing spectra, S, were acquired with different recoupling times, and the dipolar dephasing fraction $(S_0\text{-}S)/S_0$ is plotted as a function of REDOR recoupling times. The resulting ^{13}C-^{19}F REDOR dephasing curves were used for ^{13}C-^{19}F distance determination. Multiple simulated curves used for determining distances and experimental uncertainty are presented (**Figure 5**). Root-mean-square deviations (RMSDs) between the experimental and simulated REDOR values were calculated to evaluate the consistency between measurements and simulations. It is worthy to note that quantitative ssNMR distance measurements by dipolar recoupling experiments are complicated by the presence of multiple spins that couple simultaneously to each other, causing an effect known as dipolar coupling truncation[73]. In this circumstance, the recoupled dipolar coupling interaction between a two-spin pair is attenuated by the presence of nearby spins of similar or stronger couplings. In this study, due to the presence of two fluorine atoms in proximity to carbons that show REDOR dephasing, dipolar couplings of carbon to both fluorines were considered to compensate for the dipolar truncation effect. Therefore, a three-spin (^{13}C, ^{19}F and ^{19}F) system was used for most of the simulations, if not otherwise noted.

In **Figure 5A-D**, the typical ^{13}C-^{19}F REDOR dephasing curves of intra-molecular pairs (C5-F2 and C16-F1/2) and inter-molecular pairs (C23-F1 and C49/51-F1) in crystalline POSA are shown. Note that C49 and C51 resonances overlap in the 1D ^{13}C spectra. By fitting these dephasing curves, the ^{19}F-^{13}C distances were obtained: 2.7 ± 0.1 Å (C5-F2), 2.4 ± 0.3 Å (C16-F1/2), 3.3 ± 0.1 Å (C23-F1) and 4.3 ± 0.3

Å (C49/51-F1). We compared fitting results of the C5-F REDOR curve from a two-spin (^{13}C and ^{19}F) versus a three-spin (^{13}C, ^{19}F and ^{19}F) system as shown in **Figure S2**. Both simulations provided similar distance, taking into account experimental uncertainty. According to the known crystal structure[72], the C5-F1 distance is 5.7 Å, which is much longer than C5-F2 distance of 2.8 Å. When the F1 spin is far away, the C5-F2 pair can be treated as a nearly isolated spin pair. The dipolar truncation effect from a weak coupling becomes negligible. On the contrary, C16 is equidistant to two fluorines and thus the dipolar truncation effect is stronger. In the case of C49 and C51, a simulation employing a four-spin (^{13}C, ^{13}C, ^{19}F and ^{19}F) system was conducted. The distance of F1 to C49 and C51 from these fittings was approximated to be the same.

The inter-molecular distances are important for determining molecular packing of crystalline POSA. An inter-molecular packing model based on the measured distances is shown in **Figure 5E**. The proximity of F1 to C23 suggests intermolecular contacts between a difluorophenyl group and a triazole group of a neighboring molecule, which defines a "head-to-head" packing pattern. The distance of F1 in one molecule to aliphatic carbons C49 and C51 at the opposite end of another molecule implies a "head-to-tail" molecular packing in the crystal lattice. Importantly, these results of interatomic ^{13}C-^{19}F distances are in well agreement with the crystallography structure (3.3 Å for C23-F1, 4.5 Å for C49-F1 and 4.4 Å for C51-F1)[72], confirming ^{19}F-^{13}C REDOR as an accurate method to quantify atomic distances.

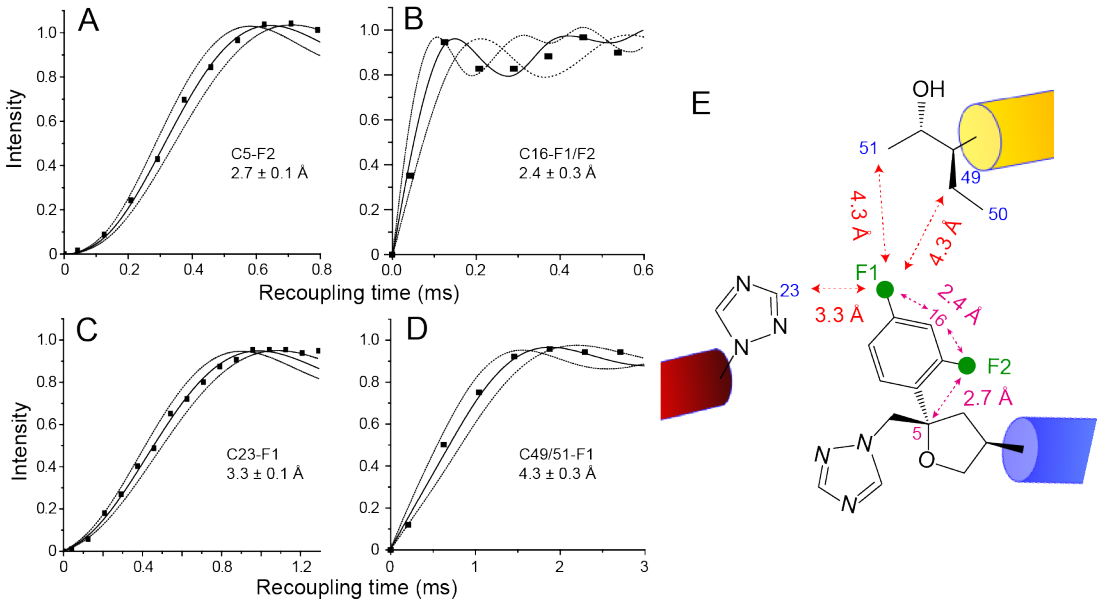

Figure 5. ^{13}C-^{19}F REDOR dephasing curves and simulations for measuring intra-molecular distances of (A) C5-F2 and (B) C16-F1/2, inter-molecular distances of (C) C23-F1 and (D) C49/51-F1 in crystalline POSA. (E) Molecular packing model of crystalline POSA derived from ^{13}C-^{19}F REDOR distances. These distances measured in ssNMR and single crystal X-ray diffraction studies match well[72].

Moreover, low NMR sensitivity due to limited natural abundance material often presents a challenge for REDOR measurements, especially nuclei pairs with long distances. The REDOR dephasing rate is slow for measuring over long distances, and therefore REDOR data of long recoupling times need to be obtained. Due to signal loss from T_2 decay, REDOR sensitivity becomes compromised at extended recoupling periods. One approach to improving sensitivity is to introduce ^{13}C isotopic labeling. Herein, ^{13}C-C44 labeled crystalline POSA was evaluated for a long-distance pair by REDOR measurements. **Figure 6A** compares direct excitation spectra of natural abundance POSA and the ^{13}C-C44 labeled POSA. The sensitivity of the C44 signal was significantly improved, which facilitated the acquisition of REDOR data. By simulating the REDOR dephasing curve in **Figure 6B**, the C44-F1 distance was determined to be 6.0 ± 0.2 Å, which corresponds to an inter-molecular contact between a difluorophenyl group and the opposite end of an adjacent molecule. This result is consistent with the distance of 6.2 Å from previous crystallography data.[72] In addition to crystalline materials, ^{13}C isotopic labeling may be useful to quantify atomic distance in amorphous materials, which usually have even lower NMR sensitivity and shorter T_2 because of the inherently disordered nature.

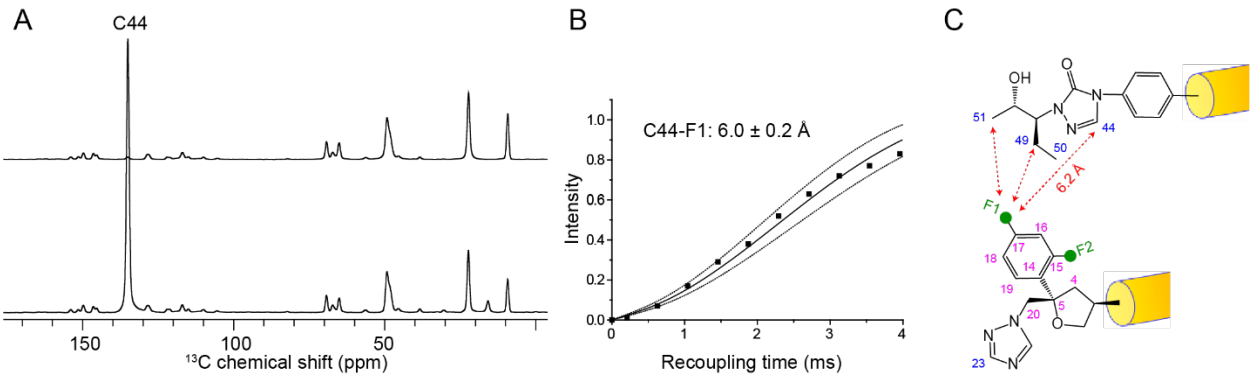

Figure 6. (A) 1D ^{13}C direct polarization (DP) spectral comparison between ^{13}C-C44 isotopically labeled and natural abundance POSA in the crystalline form. (B) REDOR dephasing curve and simulations for the determination of inter-molecular distance of C44 and fluorine atoms. (C) The inter-molecular distance of C44 and fluorine atoms representing the molecular packing of the difluorophenyl group and aliphatic carbons in crystalline POSA.

The exploration of crystalline POSA has demonstrated REDOR to be a reliable method for determining intramolecular and inter-molecular ^{13}C-^{19}F proximities. It is of interest to apply this REDOR method to explore inter-molecular interactions between drug and polymer in ASDs. Different from crystalline materials, the amorphous counterpart lacks long-range order, resulting in analytical challenges for crystallography approaches. Meanwhile, the presence of amorphous polymer in the dispersion further complicates the characterization. Therefore, both identification of drug-polymer interactions and

quantification of inter-molecular distances remain a technical challenge in pharmaceutical sciences. In the following sections, we demonstrate the application of ^{1}H-^{19}F correlation spectroscopy to qualitatively identify POSA-HPMCAS interactions and ^{13}C-^{19}F REDOR quantification of inter-molecular distances in POSA-HPMCAS dispersion at an atomic resolution.

3.3 POSA-HPMCAS Interaction Probed by 2D ^{1}H-^{19}F Correlation Spectroscopy

To probe POSA-HPMCAS interactions, 2D ^{1}H-^{19}F HETCOR correlations were utilized to identify the proximity of the ^{1}H and ^{19}F networks. **Figure 7A-C** shows a comparison between 2D ^{1}H-^{19}F HETCOR spectra of crystalline POSA, amorphous POSA, and POSA-HPMCAS amorphous solid dispersion. For crystalline POSA in **Figure 7A**, the fluorine correlations to aromatic protons at 7.5 ppm and aliphatic protons at 1.5 ppm were identified. Fluorine correlations to aliphatic protons are likely related to inter-molecular "head-to-tail" packing in crystalline POSA. A similar correlation between fluorine to aromatic protons at 7.5 ppm and aliphatic protons at 1.5 ppm was observed for amorphous POSA in **Figure 7B**. Interestingly, in the 2D ^{1}H-^{19}F HETCOR spectrum of the POSA-HPMCAS ASD, new correlations between fluorine and protons at approximately 4 ppm appeared in **Figure 7C**, where ^{1}H resonances around 4 ppm were tentatively assigned as HPMCAS hydroxyl protons. **Figure 7D** shows 1D ^{1}H cross-sections extracted from 2D ^{1}H-^{19}F HETCOR, and the new ^{1}H peak at around 4 ppm in POSA-HPMCAS dispersion is clearly evident. This ^{1}H-^{19}F correlation suggests an interaction between POSA and HPMCAS, likely between the hydroxyl group of HPMCAS and the difluorophenyl group of POSA, as shown in **Figure 7E**. Such an interaction has been previously attributed to the formation of hydrogen bond O-H···F-C between the POSA fluorine and a polymer hydroxyl group.[27] 2D ^{1}H-^{19}F hetero-nuclear correlation techniques provide direct evidence for inter-molecular contact between the POSA difluorophenyl group and polymer hydroxyl groups. However, CP-based experiments cannot quantify distances. Atomic distance measurement is needed to evaluate the interaction strength between POSA and HPMCAS in an amorphous solid dispersion.

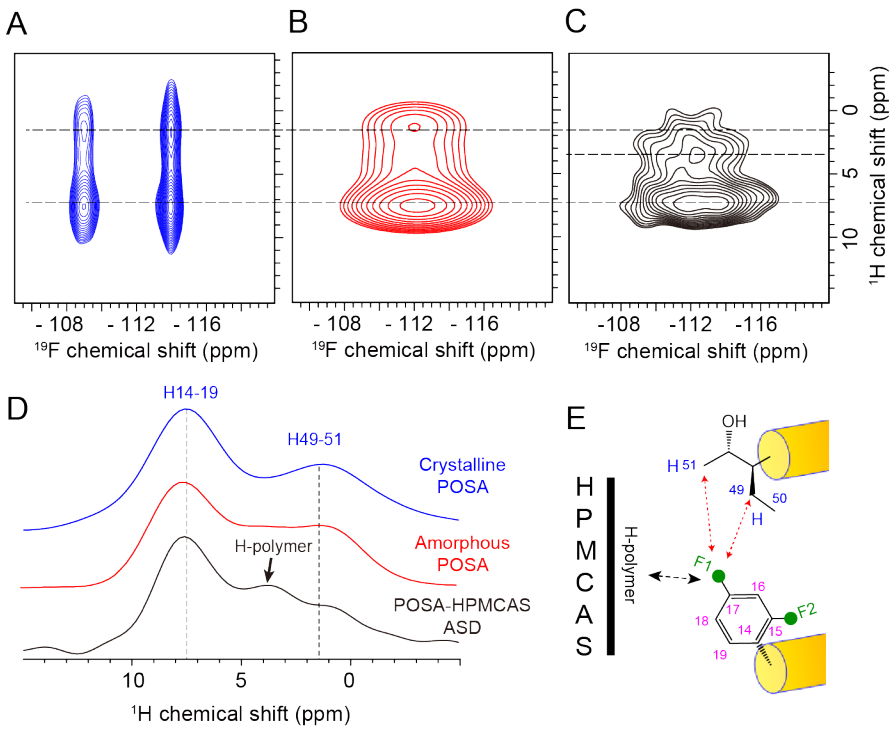

Figure 7. 2D ^{1}H-^{19}F HETCOR spectra of crystalline POSA (A), amorphous POSA (B) and POSA-HPMCAS dispersion (C). (D) 1D ^{1}H cross-sections extracted from (A) at the ^{19}F chemical shift of -114.1 ppm, -112.5 ppm and -112.5 ppm, respectively. (E) A schematic model of POSA and HPMCAS interactions showing inter-molecular interactions in amorphous POSA (red) and inter-molecular correlations observed in POSA-HPMCAS dispersion (black).

3.4 Atomic ^{19}F-^{13}C distance measurement in POSA-HPMCAS dispersions

Following the qualitative identification of a POSA-HPMCAS interaction in the ASD, we sought to utilize the REDOR method to quantify the interaction by measuring the distance from POSA fluorines to polymer carbons. **Figure 8** shows the extracted 1D REDOR dephased spectra (S) at recoupling times of 0.2 ms and 2.3 ms. Both POSA carbons (*e.g.* C50) and HPMCAS carbons (peak at 61.2 ppm) exhibit signal dephasing. Note that HPMCAS carbon at 61.2 ppm has been assigned as the carbon neighbored to the hydroxyl group.[27] At the recoupling time of 2.3 ms, the POSA C50 peak intensity decreases to *ca.* 50% in comparison to that of 0.2 ms, suggesting a close proximity to fluorine atoms. The intra-molecular distances of C50 to F1 and F2 are 19.7 Å and 20.5 Å, respectively,[72] which is too far to cause dephasing of C50 intensity. Therefore, we propose the dephasing effect is likely driven by inter-molecular "head-to-tail" packing between aliphatic protons and fluorine, as shown in **Figure 7E**. In addition, the HPMCAS carbon at 61.2 ppm exhibits 70% dephasing from 0.2 ms to 2.3 ms recoupling time, indicating an inter-molecular dipolar coupling between the POSA fluorine and the HPMCAS carbon. This faster dephasing of the HPMCAS carbon peak suggests that the distance of the POSA fluorine to the HPMCAS carbon is very likely shorter than that to the POSA C50.

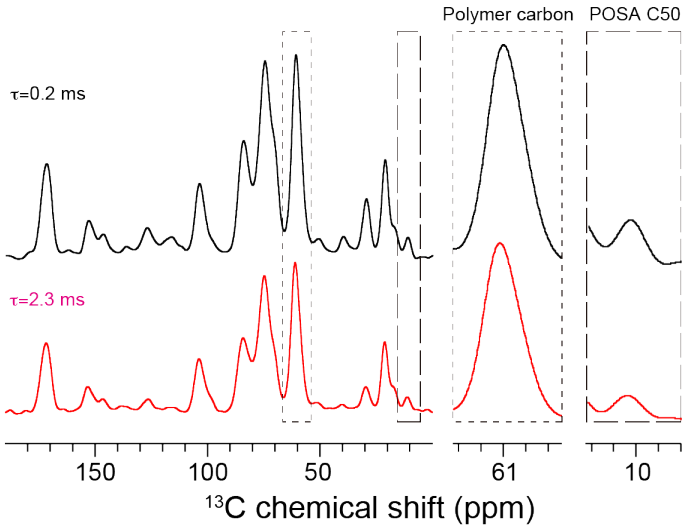

Figure 8. 1D REDOR dephased spectra of POSA-HPMCAS dispersion at dephasing times of 0.2 ms (top) and 2.3 ms (bottom). Signals of HPMCAS carbon and POSA C50 are highlighted on the right.

The REDOR dephasing curve of the HPMCAS carbon neighbored to a hydroxyl group in the POSA-HPMCAS amorphous solid dispersion is shown in **Figure 9**. To the best of our knowledge, this is the first published dataset of inter-molecular distance measurement in amorphous solid dispersions. To fit the REDOR dephasing curve, we considered different configurations of a ^{13}C-^{19}F-^{19}F three-spin system and ^{19}F chemical shift anisotropy (CSA) in the simulation. **Figure 9A-B** shows two geometries of F1 and F2 relative to a carbon atom. The intra-molecular distance of F1 and F2 is 4.67 Å, which is extracted from molecular conformation in crystalline POSA.[72] An ideal isolated C_{OH}-F1 spin pair is shown in **Figure 9A**, in which the distance of F2 to C_{OH} is the furthest and the dipolar truncation effect is the smallest. In the other extreme scenario, equal distances of fluorine atoms to carbon are considered in **Figure 9B,** resulting in the same dipolar coupling and a larger dipolar truncation effect. Both configurations were utilized for simulating ^{13}C-^{19}F REDOR data and gave $^{13}C_{OH}$-^{19}F distances of 4.3 ± 0.2 Å and 4.5 ± 0.4 Å, respectively. Thus, the dipolar truncation effect has no significant impact on the ^{13}C-^{19}F distance measurement. Such a short distance rationalizes our previous observation that ^{13}C-^{19}F CP transfer is efficient between the HPMCAS carbon and the POSA fluorine (**Figure 3**).

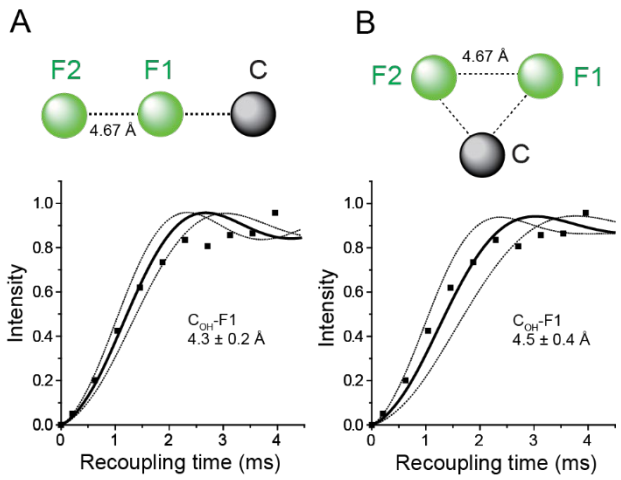

Figure 9. REDOR simulations using a three-spin (^{19}F, ^{19}F and ^{13}C) system for ^{13}C-^{19}F distance determination. (A) Straight-line and (B) triangle ^{13}C-^{19}F-^{19}F configurations.

Does the short C_{OH}-F distance indicate a strong molecular interaction in the POSA-HPMCAS dispersion? Two geometric possibilities of the relative drug and polymer orientation might result in this short C_{OH}-F distance, as shown in **Figure 10**. In the first scenario, fluorine is directly involved in the hydrogen bond O-H···F-C between HPMCAS and POSA. To simplify the calculation, the geometric influence of the sp^3 hybridization carbon (steric hindrance to the fluorine atom, resulting in $\theta \leq 109$ degree) and an O-H···F angular cutoff at > 90 degree are assumed.[74] On basis of the constant C_{OH}-F distance, a spherical coordinate system was established where the carbon next to the hydroxyl group was a fixed origin, the oxygen of the hydroxyl group was placed along the *z* axis and the hydrogen of the hydroxyl group was placed on the *x*-*z* plane. The coordinate of the fluorine atom is (r, θ, φ), where r is the radial length of C_{OH}-F distance, θ is the polar angle and φ is the azimuthal angle. As shown in **Figure 10A**, the H···F hydrogen bond distance varies with θ and φ, and ranges from 2.7 Å to 5.9 Å (C_{OH}-F distance of 4.3 Å). Given the C_{OH}-F distance of 4.5 Å, the H···F hydrogen bond distance varies from 2.9 Å to 6.1 Å while the plot is not shown here. For more details related to the calculation, see *Supporting Information*.

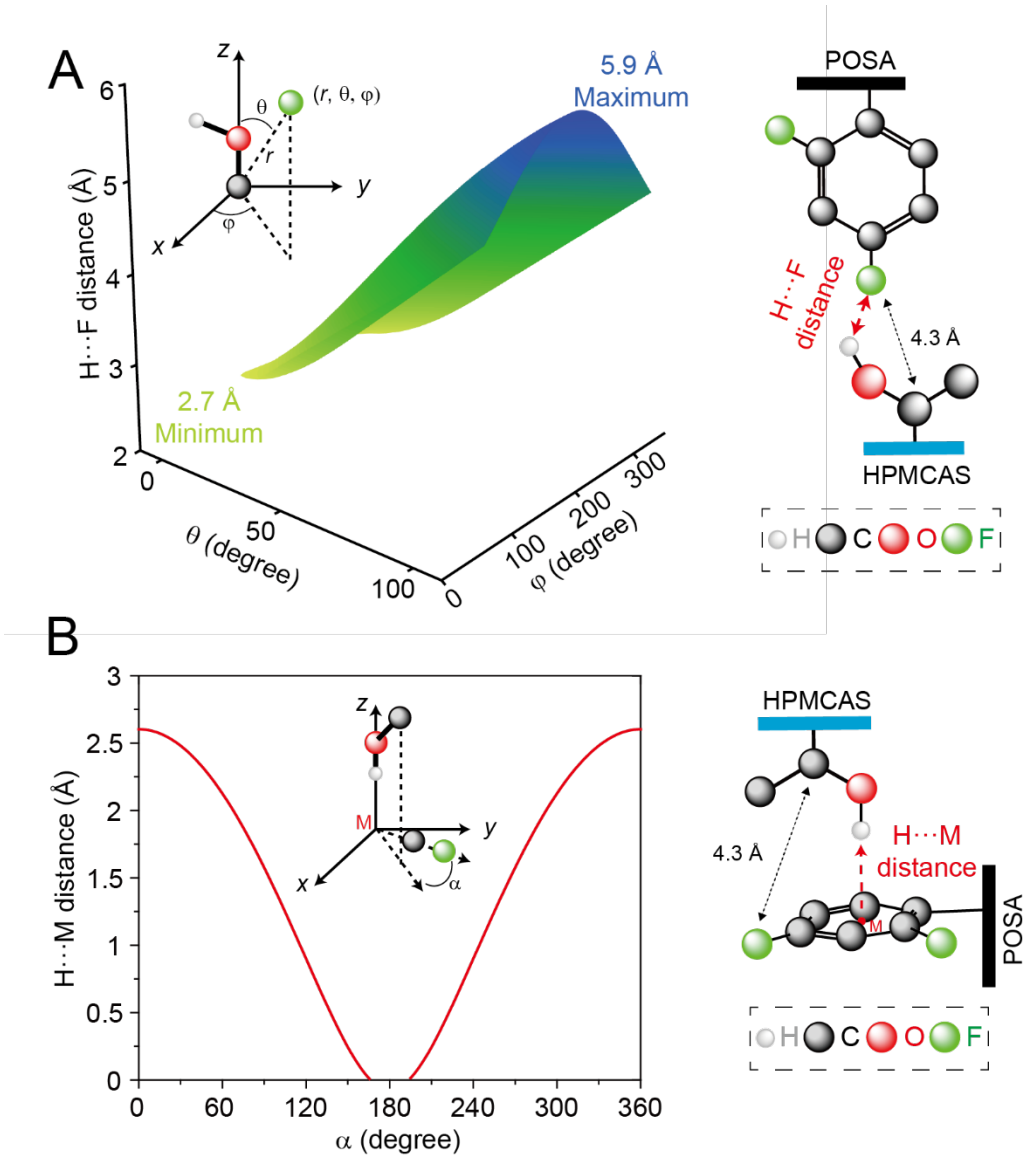

Figure 10. Two hypothetical hydrogen bonding complexes formed between POSA and HPMCAS including interaction between the polymer O-H group as an acceptor and POSA fluorine (A) or difluorophenyl ring (B) as a donor. The following geometric parameters are used: O-H covalent bond distance of 0.97 Å (typical value for alcohols by neutron diffraction),[75] C-O covalent bond distance of 1.42 Å (extracted from D-mannitol crystal),[76] C-O-H angle of 110 degree (extracted from methanol crystal by neutron diffraction),[77] C-C covalent bond distance of 1.38 Å and C-F covalent bond distance of 1.36 Å.[72]

Another possible configuration is the formation of a hydrogen bond O-H···Ph (phenyl group, π acceptor). Bond distance of hydrogen bond H···Ph is represented by H···M, where M is the center of phenyl group as shown in **Figure 10B**. To simplify the calculation, the hydroxyl group was hypothesized to be directional to the center of phenyl group, and the angle between the projection of the C-O bond on the phenyl plane and the C-F bond in the phenyl group was defined as α. **Figure 10B** shows the bond distance of H···M as a function of α, and it is within 2.6 Å when the C_{OH}-F distance is 4.3 Å. The bond distance of

H···M is up to 2.8 Å if the C_{OH}-F distance is 4.5 Å, which is not shown in **Figure 10**. The detailed calculation is provided in *Supporting Information*. It is worth noting that this calculation only considers mathematical geometries, which includes some impossible distances according to physical chemistry, *e.g.* ≤ 0 Å at α of 180^0.

4. Discussion

Exploring the molecular structure of amorphous solid dispersions is critical to predict pharmaceutical properties, including physical stability and bioavailability,[3, 7, 22, 78-80] and understanding these pharmaceutical properties can further rationalize polymer selection for ASD formulations. Consequently, an accurate measurement of intermolecular interactions is important to facilitate ASD formulation development. NMR spectroscopy can provide a versatile set of tools to enable in-depth molecular characterization of ASD microstructure. Solid-state NMR is the technique of choice in identifying inter-molecular interactions including hydrogen bond, electrostatic and dipolar interactions relevant to the physical structure of ASDs. Changes of chemical shifts provide direct evidence of new interactions formed between drugs and polymers, and local structural and motional changes.[81]

1D ^{13}C CP MAS has been used to observe molecular interactions in pharmaceutical dispersions by detecting chemical shift changes at the interaction site.[11, 13] Recently, homo- and hetero-nuclear correlation experiments were utilized to probe intermolecular interactions by detecting NMR signal transfer between the drug molecule and an excipient. In a study of its drug-polymer hydrogen bonding network[12], Nie *et al.* discovered a newly formed correlation between protonated clofazimine (CLF) and the carboxylate in hypromellose phthalate (HPMCP) in a CLF-HPMCP amorphous solid dispersion by using 2D ^{1}H-^{1}H DQ correlation experiments at 60 kHz MAS. We previously identified rich inter-molecular interactions in ASDs of POSA and HPMCAS by a combination of ^{1}H-^{13}C, ^{19}F-^{13}C, ^{15}N-^{13}C, and ^{19}F-^{1}H correlation experiments.[27] Even though the 1D and 2D ssNMR toolbox provides a straightforward and qualitative approach to characterize inter-molecular interactions in ASDs, it still lacks molecular details of the type and strength of these interactions. To determine whether new bonds are formed, inter-molecular distance measurements represent a more definitive approach in deriving molecular information about ASDs.

Based on the measured ^{13}C-^{19}F distance, two hydrogen bond patterns were proposed: O-H···F and O-H···Ph (π acceptor). As shown in **Figure 10A**, the distance of the hydrogen bond with fluorine (H···F) in the POSA-HPMCAS ASD was estimated between 2.7 Å to 5.9 Å (C_{OH}-F distance of 4.3 Å) or 2.9 Å to 6.1 Å (C_{OH}-F distance of 4.5 Å). Previously, the inter-molecular O-H···F hydrogen bond was observed in the crystalline structure of a fluorinated alcohol, which was solved by X-ray diffraction. By normalizing

the O-H covalent bond to 0.967 Å, the distance of inter-molecular H···F hydrogen bond was determined to be 2.01 Å.[82] Takemura *et al*. reported an intra-molecular O-H···F hydrogen bond in 2-fluorophenyldiphenylmethanol by X-ray crystallographic analysis, and reported the H···F intra-molecular hydrogen bond length at 2.23 Å.[83] In the Cambridge Structural Database, the mean value of the O-H···F hydrogen bond is 2.19 Å.[74] In addition, the formation of an intra-molecular O-H···F hydrogen bond was detected in 1-fluorocyclopropyl-methanol liquid by microwave spectroscopy and quantum chemical calculations.[84] The distance between the fluorine and the proton of the hydroxyl group was calculated to be as large as 2.51 Å, and regarded as a non-bonded distance because the sum of the van der Waals radii of proton and fluorine is roughly same. It is worth noting that the van der Waals radii of a proton and a fluorine (attached to phenyl group) is 1.20 Å and 1.47 Å, respectively.[85] Importantly, the calculated distance of the H···F hydrogen bond in the POSA-HPMCAS amorphous solid dispersion used in this study is at least equal or larger than the sum of the van der Waals radii of proton and fluorine, implying a fairly weak or no hydrogen bond of H···F. A similar conclusion can also be assessed from the classification of Jeffery,[86] where hydrogen bonding is a weak interaction at distances > 2.2 Å and bond angles > 90 degree.

Another possible configuration is the formation of the O-H···Ph (π acceptor) hydrogen bond. Note that bond distance of H···Ph is represented by H···M, where M is the center of phenyl group. In **Figure 10B**, the bond distance of H···M is within 2.6 Å (C_{OH}-F distance of 4.3 Å) or up to 2.8 Å (C_{OH}-F distance of 4.5 Å). Different from the rare occurrence of the O-H···F hydrogen bond in Cambridge Structural Database, many materials have been reported to form O-H···Ph (π acceptor) hydrogen bonds and the mean value is reported to be 2.50 Å.[74] For example, an inter-molecular hydrogen bond is formed between the OH group and the phenyl group in a 2,2,2-trifluoro-1-(9-anthryl)ethanol crystal, and the proton was found to be 2.2 Å away from phenyl group place.[87] A similar inter-molecular O-H···Ph hydrogen bond was found in tetraphenylborate salts, and the H···Ph bond length was reported as 2.17 Å.[88] Therefore, we propose that the O-H···Ph hydrogen bond between POSA and HPMCAS is likely present in the POSA-HPMCAS amorphous solid dispersion. Considering the complex nature of amorphous solid dispersion structures, two types of hydrogen bond might co-exist. Reimann *et al*. studied the co-existence of O-H···Ph and O-H···F in clusters of fluorobenzene and fluoroform using infrared ion-depletion spectroscopy and ab initio calculations.[89]

The quantification of inter-molecular distance allows us to discover possible interactions between POSA and HPMCAS through O-H···F and O-H···Ph hydrogen bonds. To further confirm the existence of such interactions, more distance restraints are required. The advancement of MAS NMR in the past many years has offered a great potential to elucidate molecular details in pharmaceutical amorphous materials.

For example, $^{17}O\cdots^{1}H$ distance measurements by REDOR have been used to determine the strength of hydrogen bonding between two adjacent L-tyrosine molecules.[63] The distance of $^{15}N\cdots^{1}H$ as a signature of hydrogen bonding in 1,8-bis(dimethylamino)naphthalene was measured using a 2D ^{15}N-^{1}H dipolar chemical-shift (DIPSHIFT) correlation experiment.[90] The strength of ^{1}H-^{19}F dipole-dipole coupling for measuring H···F hydrogen bond has been carried out in fluorinated organic molecules.[91] Most recently, hydrogen bonding in the deep eutectic Lidocaine-Ibuprofen formulation has been identified using Nuclear Overhauser Effect (NOE) build-up curves.[92] Histidine N-H bond lengths can be efficienty measured by frequency selective heteronuclear multiple quantum coherence (HMQC) and resonance echo saturation pulse double resonance (RESPDOR) experiments.[93] Moreover, our previous study has suggested a rich category of POSA and HPMCAS interactions in the ASD.[27] It will be interesting to further uncover the nature of these interactions by identifying the inter-atomic proximity. Therefore, development and utilization of inter-molecular distance measurements by MAS NMR has the potential to improve the structural characterization of ASDs at a molecular level and to facilitate the rational design of ASD formulations.

5. Conclusion

In this study, we demonstrated the first example of quantitative measurement of drug-polymer interactions in a POSA-HPMCAS amorphous solid dispersion. The ^{19}F-^{13}C cross polarization build-up curves were utilized to carry out semi-qualitative distance analysis in crystalline POSA, and a variant ^{19}F-^{13}C Rotational Echo and Double Resonance (REDOR) technique was used to successfully identify the structural details of crystalline POSA, including “head-to-head” and “head-to-tail” packings. The distances measured by REDOR in crystalline POSA are consistent with crystallographic data, making REDOR an accurate method to quantify molecular distances. Furthermore, the inter-molecular interactions in the POSA-HPMCAS amorphous solid dispersion were qualitatively analyzed by 2D ^{1}H-^{19}F HETCOR, and a correlation between the hydroxyl group of HPMCAS and the difluorophenyl group of POSA was assigned. Such interaction was further investigated by a ^{19}F-^{13}C REDOR method. By utilizing different spin systems in REDOR simulation, we quantified the distance between ^{13}C of the HPMCAS hydroxyl group and ^{19}F of POSA as 4.3 ± 0.2 Å or 4.5 ± 0.4 Å. With the aid of geometric calculations, two hydrogen bond patterns (O-H···F and O-H···Ph) were proposed. This work represents the first direct atomic distance measurement of amorphous solid dispersions. It also demonstrates the REDOR technique as a powerful tool for investigating molecular details of drug-polymer interactions and providing a structural basis for polymer selection during development of amorphous solid dispersions.

6. Acknowledgment

X. L. and M. L. are grateful to MRL Postdoctoral Research Program. L. Y. acknowledges NSF support through the University of Wisconsin Materials Research Science and Engineering Center (Grant DMR-1720415). The authors would like to thank Dr. Dirk Stueber (Merck & Co, Inc) for his helpful discussions.

7. Reference

1. Benet, L. Z. The Role of BCS (Biopharmaceutics Classification System) and BDDCS (Biopharmaceutics Drug Disposition Classification System) in Drug Development. *Journal of Pharmaceutical Sciences* **2013,** *102*, (1), 34-42.
2. Taylor, L. S.; Zhang, G. G. Z. Physical chemistry of supersaturated solutions and implications for oral absorption. *Advanced Drug Delivery Reviews* **2016,** *101*, 122-142.
3. Que, C.; Lou, X.; Zemlyanov, D. Y.; Mo, H.; Indulkar, A. S.; Gao, Y.; Zhang, G. G. Z.; Taylor, L. S. Insights into the Dissolution Behavior of Ledipasvir–Copovidone Amorphous Solid Dispersions: Role of Drug Loading and Intermolecular Interactions. *Molecular pharmaceutics* **2019,** *16*, (12), 5054-5067.
4. Sarode, A. L.; Sandhu, H.; Shah, N.; Malick, W.; Zia, H. Hot melt extrusion (HME) for amorphous solid dispersions: Predictive tools for processing and impact of drug–polymer interactions on supersaturation. *European Journal of Pharmaceutical Sciences* **2013,** *48*, (3), 371-384.
5. Ahlneck, C.; Zografi, G. The Molecular-Basis of Moisture Effects on the Physical and Chemical-Stability of Drugs in the Solid-State. *International Journal of Pharmaceutics* **1990,** *62*, (2-3), 87-95.
6. Huang, C.; Powell, C. T.; Sun, Y.; Cai, T.; Yu, L. Effect of Low-Concentration Polymers on Crystal Growth in Molecular Glasses: A Controlling Role for Polymer Segmental Mobility Relative to Host Dynamics. *The Journal of Physical Chemistry B* **2017,** *121*, (8), 1963-1971.
7. Yao, X.; Huang, C.; Benson, E. G.; Shi, C.; Zhang, G. G. Z.; Yu, L. Effect of Polymers on Crystallization in Glass-Forming Molecular Liquids: Equal Suppression of Nucleation and Growth and Master Curve for Prediction. *Crystal Growth & Design* **2019**.
8. Saboo, S.; Kestur, U. S.; Flaherty, D. P.; Taylor, L. S. Congruent release of drug and polymer from amorphous solid dispersions: insights into the role of drug-polymer hydrogen bonding, surface crystallization and glass transition. *Molecular pharmaceutics* **2020**.
9. Kothari, K.; Ragoonanan, V.; Suryanarayanan, R. The Role of Drug–Polymer Hydrogen Bonding Interactions on the Molecular Mobility and Physical Stability of Nifedipine Solid Dispersions. *Molecular pharmaceutics* **2015,** *12*, (1), 162-170.
10. Maniruzzaman, M.; Pang, J.; Morgan, D. J.; Douroumis, D. Molecular Modeling as a Predictive Tool for the Development of Solid Dispersions. *Molecular pharmaceutics* **2015,** *12*, (4), 1040-1049.
11. Mistry, P.; Mohapatra, S.; Gopinath, T.; Vogt, F. G.; Suryanarayanan, R. Role of the Strength of Drug–Polymer Interactions on the Molecular Mobility and Crystallization Inhibition in Ketoconazole Solid Dispersions. *Molecular pharmaceutics* **2015,** *12*, (9), 3339-3350.
12. Nie, H.; Su, Y.; Zhang, M.; Song, Y.; Leone, A.; Taylor, L. S.; Marsac, P. J.; Li, T.; Byrn, S. R. Solid-State Spectroscopic Investigation of Molecular Interactions between Clofazimine and Hypromellose Phthalate in Amorphous Solid Dispersions. *Molecular pharmaceutics* **2016,** *13*, (11), 3964-3975.
13. Song, Y.; Yang, X.; Chen, X.; Nie, H.; Byrn, S.; Lubach, J. W. Investigation of Drug–Excipient Interactions in Lapatinib Amorphous Solid Dispersions Using Solid-State NMR Spectroscopy. *Molecular pharmaceutics* **2015,** *12*, (3), 857-866.
14. Yani, Y.; Kanaujia, P.; Chow, P. S.; Tan, R. B. H. Effect of API-Polymer Miscibility and Interaction on the Stabilization of Amorphous Solid Dispersion: A Molecular Simulation Study. *Industrial & Engineering Chemistry Research* **2017,** *56*, (44), 12698-12707.
15. Paudel, A.; Meeus, J.; Mooter, G., Structural characterization of amorphous solid dispersions. In *Amorphous solid dispersions, advances in delivery science and technology*, Shah, N.; Sandhu, H.; Choi, D.; Chokshi, H.; Malick, A., Eds. Springer, New York, NY : 2014.

16. Shah, B.; Kakumanu, V. K.; Bansal, A. K. Analytical techniques for quantification of amorphous/crystalline phases in pharmaceutical solids. *Journal of Pharmaceutical Sciences* **2006,** *95*, (8), 1641-1665.
17. Ricarte, R. G.; Lodge, T. P.; Hillmyer, M. A. Detection of Pharmaceutical Drug Crystallites in Solid Dispersions by Transmission Electron Microscopy. *Molecular pharmaceutics* **2015,** *12*, (3), 983-990.
18. Lamm, M. S.; Simpson, A.; McNevin, M.; Frankenfeld, C.; Nay, R.; Variankaval, N. Probing the Effect of Drug Loading and Humidity on the Mechanical Properties of Solid Dispersions with Nanoindentation: Antiplasticization of a Polymer by a Drug Molecule. *Molecular pharmaceutics* **2012,** *9*, (11), 3396-3402.
19. Taylor, L. S.; Zografi, G. Spectroscopic Characterization of Interactions Between PVP and Indomethacin in Amorphous Molecular Dispersions. *Pharmaceutical Research* **1997,** *14*, (12), 1691-1698.
20. Taylor, L. S.; Zografi, G. Sugar–polymer hydrogen bond interactions in lyophilized amorphous mixtures. *Journal of Pharmaceutical Sciences* **1998,** *87*, (12), 1615-1621.
21. Que, C. L.; Lou, X. C.; Zemlyanov, D. Y.; Mo, H. P.; Indulkar, A. S.; Gao, Y.; Zhang, G. G. Z.; Taylor, L. S. Insights into the Dissolution Behavior of Ledipasvir-Copovidone Amorphous Solid Dispersions: Role of Drug Loading and Intermolecular Interactions. *Molecular pharmaceutics* **2019,** *16*, (12), 5054-5067.
22. Marsac, P. J.; Rumondor, A. C. F.; Nivens, D. E.; Kestur, U. S.; Stanciu, L.; Taylor, L. S. Effect of temperature and moisture on the miscibility of amorphous dispersions of felodipine and poly(vinyl pyrrolidone). *Journal of Pharmaceutical Sciences* **2010,** *99*, (1), 169-185.
23. Meng, F.; Trivino, A.; Prasad, D.; Chauhan, H. Investigation and correlation of drug polymer miscibility and molecular interactions by various approaches for the preparation of amorphous solid dispersions. *European Journal of Pharmaceutical Sciences* **2015,** *71*, 12-24.
24. de Araujo, G. L. B.; Benmore, C. J.; Byrn, S. R. Local Structure of Ion Pair Interaction in Lapatinib Amorphous Dispersions characterized by Synchrotron X-Ray diffraction and Pair Distribution Function Analysis. *Scientific Reports* **2017,** *7*, 46367.
25. Sarpal, K.; Delaney, S.; Zhang, G. G. Z.; Munson, E. J. Phase Behavior of Amorphous Solid Dispersions of Felodipine: Homogeneity and Drug-Polymer Interactions. *Molecular pharmaceutics* **2019**.
26. Ishizuka, Y.; Ueda, K.; Okada, H.; Takeda, J.; Karashima, M.; Yazawa, K.; Higashi, K.; Kawakami, K.; Ikeda, Y.; Moribe, K. Effect of Drug-Polymer Interactions through Hypromellose Acetate Succinate Substituents on the Physical Stability on Solid Dispersions Studied by Fourier-Transform Infrared and Solid-State Nuclear Magnetic Resonance. *Molecular pharmaceutics* **2019,** *16*, (6), 2785-2794.
27. Lu, X. Y.; Huang, C. B.; Lowinger, M. B.; Yang, F. Y.; Xu, W.; Brown, C. D.; Hesk, D.; Koynov, A.; Schenck, L.; Su, Y. C. Molecular Interactions in Posaconazole Amorphous Solid Dispersions from Two-Dimensional Solid-State NMR Spectroscopy. *Molecular pharmaceutics* **2019,** *16*, (6), 2579-2589.
28. Vogt, F. G.; Roberts-Skilton, K.; Kennedy-Gabb, S. A. A Solid-State NMR Study of Amorphous Ezetimibe Dispersions in Mesoporous Silica. *Pharmaceutical Research* **2013,** *30*, (9), 2315-2331.
29. Abraham, A.; Crull, G. Understanding API-Polymer Proximities in Amorphous Stabilized Composite Drug Products Using Fluorine-Carbon 2D HETCOR Solid-State NMR. *Molecular pharmaceutics* **2014,** *11*, (10), 3754-3759.
30. Fortier-McGill, B.; Toader, V.; Reven, L. H-1 Solid State NMR Study of Poly(methacrylic acid) Hydrogen-Bonded Complexes. *Macromolecules* **2012,** *45*, (15), 6015-6026.
31. Io, T.; Fukami, T.; Yamamoto, K.; Suzuki, T.; Xu, J.; Tomono, K.; Ramamoorthy, A. Homogeneous nanoparticles to enhance the efficiency of a hydrophobic drug, antihyperlipidemic probucol, characterized by solid-state NMR. *Molecular pharmaceutics* **2010,** *7*, (1), 299-305.
32. Pan, Y.; Gullion, T.; Schaefer, J. Determination of C-N Internuclear Distances by Rotational-Echo Double-Resonance Nmr of Solids. *Journal of Magnetic Resonance* **1990,** *90*, (2), 330-340.
33. Herzog, K.; Thomas, B.; Sprenger, D.; Jager, C. Redor Nmr - Approaching Structural Elucidation of Hydrated Layers in Silicate Electrode Glasses. *Journal of Non-Crystalline Solids* **1995,** *190*, (3), 296-300.

34. Gullion, T. Recent Applications of REDOR to Biological Problems. *Annual Reports on Nmr Spectroscopy, Vol 65* **2009,** *65*, 111-137.
35. Cegelski, L. REDOR NMR for drug discovery. *Bioorganic & Medicinal Chemistry Letters* **2013,** *23*, (21), 5767-5775.
36. J., G. T. S. Rotational-echo double-resonance NMR. *J Magn Reson* **1989,** *81*, 5.
37. Kim, S. J.; Cegelski, L.; Preobrazhenskaya, M.; Schaefer, J. Structures of Staphylococcus aureus cell-wall complexes with vancomycin, eremomycin, and chloroeremomycin derivatives by C-13{F-19} and N-15{F-19} rotational-echo double resonance. *Biochemistry* **2006,** *45*, (16), 5235-5250.
38. Sack, I.; Goldbourt, A.; Vega, S.; Buntkowsky, G. Deuterium REDOR: Principles and applications for distance measurements. *Journal of Magnetic Resonance* **1999,** *138*, (1), 54-65.
39. Mani, R.; Tang, M.; Wu, X.; Buffy, J. J.; Waring, A. J.; Sherman, M. A.; Hong, M. Membrane-bound dimer structure of a beta-hairpin antimicrobial peptide from rotational-echo double-resonance solid-state NMR. *Biochemistry* **2006,** *45*, (27), 8341-9.
40. Mani, R.; Cady, S. D.; Tang, M.; Waring, A. J.; Lehrer, R. I.; Hong, M. Membrane-dependent oligomeric structure and pore formation of a beta-hairpin antimicrobial peptide in lipid bilayers from solid-state NMR. *Proc Natl Acad Sci U S A* **2006,** *103*, (44), 16242-7.
41. Ghosh, M.; Rienstra, C. M. H-1-Detected REDOR with Fast Magic-Angle Spinning of a Deuterated Protein. *Journal of Physical Chemistry B* **2017,** *121*, (36), 8503-8511.
42. Graesser, D. T.; Wylie, B. J.; Nieuwkoop, A. J.; Franks, W. T.; Rienstra, C. M. Long-range F-19-N-15 distance measurements in highly-C-13, N-15-enriched solid proteins with F-19-dephased REDOR shift (FRESH) spectroscopy. *Magnetic Resonance in Chemistry* **2007,** *45*, S129-S134.
43. Goetz, J. M.; Poliks, B.; Studelska, D. R.; Fischer, M.; Kugelbrey, K.; Bacher, A.; Cushman, M.; Schaefer, J. Investigation of the binding of fluorolumazines to the 1-MDa capsid of lumazine synthase by N-15{F-19} REDOR NMR. *Journal of the American Chemical Society* **1999,** *121*, (33), 7500-7508.
44. Lee, J. H.; Kim, M. S.; Lee, H. W.; Lee, I. Y. C.; Kim, H. K.; Kim, N. D.; Lee, S.; Seo, H.; Paik, Y. The Application of REDOR NMR to Understand the Conformation of Epothilone B. *International Journal of Molecular Sciences* **2017,** *18*, (7).
45. Cady, S.; Wang, T.; Hong, M. Membrane-Dependent Effects of a Cytoplasmic Helix on the Structure and Drug Binding of the Influenza Virus M2 Protein. *Journal of the American Chemical Society* **2011,** *133*, (30), 11572-11579.
46. Grage, S. L.; Watts, J. A.; Watts, A. H-2{F-19} REDOR for distance measurements in biological solids using a double resonance spectrometer. *Journal of Magnetic Resonance* **2004,** *166*, (1), 1-10.
47. Wang, J.; Sanchez-Rosello, M.; Acena, J. L.; del Pozo, C.; Sorochinsky, A. E.; Fustero, S.; Soloshonok, V. A.; Liu, H. Fluorine in Pharmaceutical Industry: Fluorine-Containing Drugs Introduced to the Market in the Last Decade (2001-2011). *Chemical Reviews* **2014,** *114*, (4), 2432-2506.
48. Rowe, R. C.; Sheskey, P. J.; Quinn, M. E.; Association, A. P., *Handbook of Pharmaceutical Excipients*. Pharmaceutical Press: 2009.
49. Lee, Y. J.; Clark, C. G., Jr.; Graf, R.; Wagner, M.; Mullen, K.; Spiess, H. W. Solid-state organization of semifluorinated alkanes probed by 19F MAS NMR spectroscopy. *J Phys Chem B* **2009,** *113*, (5), 1360-6.
50. Wang, W. D.; Gao, X. D.; Strohmeier, M.; Wang, W.; Bai, S.; Dybowski, C. Solid-State NMR Studies of Form I of Atorvastatin Calcium. *Journal Of Physical Chemistry B* **2012,** *116*, (11), 3641-3649.
51. Lu, X.; Skomski, D.; Thompson, K. C.; McNevin, M. J.; Xu, W.; Su, Y. Three-Dimensional NMR Spectroscopy of Fluorinated Pharmaceutical Solids under Ultrafast Magic Angle Spinning. *Anal Chem* **2019,** *91*, (9), 6217-6224.
52. Shcherbakov, A. A.; Hong, M. Rapid measurement of long-range distances in proteins by multidimensional (13)C-(19)F REDOR NMR under fast magic-angle spinning. *J Biomol NMR* **2018,** *71*, (1), 31-43.
53. Wi, S.; Sinha, N.; Hong, M. Long-range 1H-19F distance measurement in peptides by solid-state NMR. *J Am Chem Soc* **2004,** *126*, (40), 12754-5.

54. Hagaman, E. W.; Burns, J. H. The Determination Of Local-Structure In Organofluorides Using F-19 C-13 Dipolar Coupling. *Fuel* **1993,** *72*, (8), 1239-1243.
55. Kim, S. J.; Cegelski, L.; Preobrazhenskaya, M.; Schaefer, J. Structures of Staphylococcus aureus cell-wall complexes with vancomycin, eremomycin, and chloroeremomycin derivatives by 13C{19F} and 15N{19F} rotational-echo double resonance. *Biochemistry* **2006,** *45*, (16), 5235-50.
56. Olsen, G. L.; Louie, E. A.; Drobny, G. P.; Sigurdsson, S. T. Determination of DNA minor groove width in distamycin-DNA complexes by solid-state NMR. *Nucleic Acids Res* **2003,** *31*, (17), 5084-9.
57. Louie, E. A.; Chirakul, P.; Raghunathan, V.; Sigurdsson, S. T.; Drobny, G. P. Using solid-state P-31{F-19} REDOR NMR to measure distances between a trifluoromethyl group and a phosphodiester in nucleic acids. *Journal of Magnetic Resonance* **2006,** *178*, (1), 11-24.
58. Graesser, D. T.; Wylie, B. J.; Nieuwkoop, A. J.; Franks, W. T.; Rienstra, C. M. Long-range 19F-15N distance measurements in highly-13C, 15N-enriched solid proteins with 19F-dephased REDOR shift (FRESH) spectroscopy. *Magn Reson Chem* **2007,** *45 Suppl 1*, S129-34.
59. Lu, X. Y.; Lafon, O.; Trebosc, J.; Amoureux, J. P. Detailed analysis of the S-RESPDOR solid-state NMR method for inter-nuclear distance measurement between spin-1/2 and quadrupolar nuclei. *Journal Of Magnetic Resonance* **2012,** *215*, 34-49.
60. Chen, L.; Wang, Q. A.; Hu, B. W.; Lafon, O.; Trebosc, J.; Deng, F.; Amoureux, J. P. Measurement of hetero-nuclear distances using a symmetry-based pulse sequence in solid-state NMR. *Physical Chemistry Chemical Physics* **2010,** *12*, (32), 9395-9405.
61. Goetz, J. M.; Schaefer, J. REDOR dephasing by multiple spins in the presence of molecular motion. *J Magn Reson* **1997,** *127*, (2), 147-54.
62. Wang, Q. A.; Lu, X. Y.; Lafon, O.; Trebosc, J.; Deng, F.; Hu, B. W.; Chen, Q.; Amoureux, J. P. Measurement of C-13-H-1 dipolar couplings in solids by using ultra-fast magic-angle spinning NMR spectroscopy with symmetry-based sequences. *Physical Chemistry Chemical Physics* **2011,** *13*, (13), 5967-5973.
63. Brinkmann, A.; Kentgens, A. P. Proton-selective 17O-1H distance measurements in fast magic-angle-spinning solid-state NMR spectroscopy for the determination of hydrogen bond lengths. *J Am Chem Soc* **2006,** *128*, (46), 14758-9.
64. Bak, M.; Rasmussen, J. T.; Nielsen, N. C. SIMPSON: a general simulation program for solid-state NMR spectroscopy. *J Magn Reson* **2000,** *147*, (2), 296-330.
65. Nie, H. C.; Su, Y. C.; Zhang, M. T.; Song, Y.; Leone, A.; Taylor, L. S.; Marsac, P. J.; Li, T. L.; Byrn, S. R. Solid-State Spectroscopic Investigation of Molecular Interactions between Clofazimine and Hypromellose Phthalate in Amorphous Solid Dispersions. *Molecular pharmaceutics* **2016,** *13*, (11), 3964-3975.
66. Song, Y.; Yang, X. H.; Chen, X.; Nie, H. C.; Byrn, S.; Lubach, J. W. Investigation of Drug-Excipient Interactions in Lapatinib Amorphous Solid Dispersions Using Solid-State NMR Spectroscopy. *Molecular pharmaceutics* **2015,** *12*, (3), 857-866.
67. Mistry, P.; Mohapatra, S.; Gopinath, T.; Vogt, F. G.; Suryanarayanan, R. Role of the Strength of Drug-Polymer Interactions on the Molecular Mobility and Crystallization Inhibition in Ketoconazole Solid Dispersions. *Molecular pharmaceutics* **2015,** *12*, (9), 3339-3350.
68. Kothari, K.; Ragoonanan, V.; Suryanarayanan, R. The Role of Drug-Polymer Hydrogen Bonding Interactions on the Molecular Mobility and Physical Stability of Nifedipine Solid Dispersions. *Molecular pharmaceutics* **2015,** *12*, (1), 162-170.
69. Lu, X.; Xu, W.; Hanada, M.; Jermain, S. V.; Williams, R. O., 3rd; Su, Y. Solid-state NMR analysis of crystalline and amorphous Indomethacin: An experimental protocol for full resonance assignments. *J Pharm Biomed Anal* **2019,** *165*, 47-55.
70. Giraudet, J.; Dubois, M.; Guerin, K.; Delabarre, C.; Pirotte, P.; Hamwi, A.; Masin, F. Heteronuclear dipolar recoupling using Hartmann-Hahn cross polarization: a probe for 19F-13C distance determination of fluorinated carbon materials. *Solid State Nucl Magn Reson* **2007,** *31*, (3), 131-40.

71. Giraudet, J.; Dubois, M.; Hamwi, A.; Stone, W. E.; Pirotte, P.; Masin, F. Solid-state NMR (19F and 13C) study of graphite monofluoride (CF)n: 19F spin-lattice magnetic relaxation and 19F/13C distance determination by Hartmann-Hahn cross polarization. *J Phys Chem B* **2005,** *109*, (1), 175-81.
72. McQuiston, D. K.; Mucalo, M. R.; Saunders, G. C. The structure of posaconazole and its solvates with methanol, and dioxane and water: Difluorophenyl as a hydrogen bond donor. *Journal Of Molecular Structure* **2019,** *1179*, 477-486.
73. Bayro, M. J.; Huber, M.; Ramachandran, R.; Davenport, T. C.; Meier, B. H.; Ernst, M.; Griffin, R. G. Dipolar truncation in magic-angle spinning NMR recoupling experiments. *J Chem Phys* **2009,** *130*, (11), 114506.
74. Steiner, T. The Hydrogen Bond in the Solid State. *Angewandte Chemie International Edition* **2002,** *41*, (1), 48-76.
75. Allen, F. H.; Kennard, O.; Watson, D. G.; Brammer, L.; Orpen, A. G.; Taylor, R. Tables of bond lengths determined by X-ray and neutron diffraction. Part 1. Bond lengths in organic compounds. *Journal of the Chemical Society, Perkin Transactions 2* **1987**, (12), S1-S19.
76. Fronczek, F. R.; Kamel, H. N.; Slattery, M. Three polymorphs ([alpha], [beta], and [delta]) of d-mannitol at 100 K. *Acta Crystallographica Section C* **2003,** *59*, (10), o567-o570.
77. Torrie, B. H.; Weng, S. X.; Powell, B. M. Structure of the α-phase of solid methanol. *Molecular Physics* **1989,** *67*, (3), 575-581.
78. Wegiel, L. A.; Mauer, L. J.; Edgar, K. J.; Taylor, L. S. Crystallization of amorphous solid dispersions of resveratrol during preparation and storage-Impact of different polymers. *Journal of Pharmaceutical Sciences* **2013,** *102*, (1), 171-184.
79. Vogt, F. G. Evolution of solid-state NMR in pharmaceutical analysis. *Future Medicinal Chemistry* **2010,** *2*, (6), 915-921.
80. Skorupska, E.; Jeziorna, A.; Kazmierski, S.; Potrzebowski, M. J. Recent progress in solid-state NMR studies of drugs confined within drug delivery systems. *Solid State Nuclear Magnetic Resonance* **2014,** *57-58*, 2-16.
81. Berendt, R. T.; Sperger, D. M.; Isbester, P. K.; Munson, E. J. Solid-state NMR spectroscopy in pharmaceutical research and analysis. *Trac-Trends in Analytical Chemistry* **2006,** *25*, (10), 977-984.
82. Barbarich, T. J.; Rithner, C. D.; Miller, S. M.; Anderson, O. P.; Strauss, S. H. Significant Inter- and Intramolecular O−H···FC Hydrogen Bonding. *Journal of the American Chemical Society* **1999,** *121*, (17), 4280-4281.
83. Takemura, H.; Kaneko, M.; Sako, K.; Iwanaga, T. The intramolecular C–F···HO hydrogen bond of 2-fluorophenyldiphenylmethanol. *New Journal of Chemistry* **2009,** *33*, (10), 2004-2006.
84. Mollendal, H.; Leonov, A.; de Meijere, A. Intramolecular hydrogen bonding in (1-fluorocyclopropyl)methanol as studied by microwave spectroscopy and quantum chemical calculations. *Journal of Molecular Structure* **2004,** *695*, 163-169.
85. Bondi, A. van der Waals Volumes and Radii. *The Journal of Physical Chemistry* **1964,** *68*, (3), 441-451.
86. Jeffrey, G. A., *An Introduction to Hydrogen Bonding*. Oxford University Press: 1997.
87. Rzepa, H. S.; Webb, M. L.; Slawin, A. M. Z.; Williams, D. J. π Facial hydrogen bonding in the chiral resolving agent (S)-2,2,2-trifluoro-1-(9-anthryl)ethanol and its racemic modification. *Journal of the Chemical Society, Chemical Communications* **1991**, (11), 765-768.
88. Steiner, T.; Schreurs, A. M. M.; Lutz, M.; Kroon, J. Making very short O–H···Ph hydrogen bonds: the example of tetraphenylborate salts. *New Journal of Chemistry* **2001,** *25*, (1), 174-178.
89. Reimann, B.; Buchhold, K.; Vaupel, S.; Brutschy, B.; Havlas, Z.; Špirko, V.; Hobza, P. Improper, Blue-Shifting Hydrogen Bond between Fluorobenzene and Fluoroform. *The Journal of Physical Chemistry A* **2001,** *105*, (23), 5560-5566.
90. White, P. B.; Hong, M. (15)N and (1)H Solid-State NMR Investigation of a Canonical Low-Barrier Hydrogen-Bond Compound: 1,8-Bis(dimethylamino)naphthalene. *J Phys Chem B* **2015,** *119*, (35), 11581-9.

91. Althoff, G.; Ruiz, J.; Rodriguez, V.; Lopez, G.; Perez, J.; Janiak, C. Can a single C-H center dot center dot center dot F-C hydrogen bond make a difference? Assessing the H center dot center dot center dot F bond strength from 2-D H-1-F-19 CP/MAS NMR. *Crystengcomm* **2006,** *8*, (9), 662-665.
92. Mann, S. K.; Pham, T. N.; McQueen, L, L., Lewandowski, J. R.; Brown, S. P. Revealing Intermolecular Hydrogen Bonding Structure and Dynamics in a Deep Eutectic Pharmaceutical by Magic-Angle Spinning NMR Spectroscopy, *Mol. Pharmaceutics* **2020**, 17, 2, 622-631
93. Wijesekara, A.V.; Venkatesh, A.; Lampkin, B.J.; VanVeller, B.; Lubach, J.W.;, Nagapudi, K.; Hung, I.; Gor'kov, P.L.; Gan, Z.; Rossini, A.J. Fast Acquisition of Proton Detected HETCOR Solid-State NMR Spectra of Quadrupolar Nuclei and Rapid Measurement of NH Bond Lengths by Frequency Selective HMQC and RESPDOR Pulse Sequences, *Chemistry* **2020,** Epub ahead of print